Mathematical and Computational Applications

MDPI

Article

A Novel Second-Order Total Variation Model with Biharmonic for High-Quality Image Inpainting

Ahmed K. Al-Jaberi [1,*], Alina Alb Lupas [2,*] and Daria Lupas [3]

[1] Department of Mathematics, College of Education for Pure Science, University of Basrah, Basrah 61004, Iraq
[2] Department of Mathematics and Computer Science, University of Oradea, 1 Universitatii Street, 410087 Oradea, Romania
[3] Faculty of Construction, Cadastre and Architecture, University of Oradea, 410087 Oradea, Romania; darialupas@gmail.com
* Correspondence: ahmed.shanan@uobasrah.edu.iq (A.K.A.-J.); dalb@uoradea.ro (A.A.L.)

Abstract

Image reconstruction aims to restore missing parts of the image while keeping geometry and quality intact. The traditional second-order partial differential equation (PDE) and Total Variation (TV) methods can be used to perform such an action; nonetheless, their disadvantages, such as over-smoothing, staircase effect, and loss of cornerstones in image details, have been noted. The major disadvantages of those approaches led to the idea of developing a second-order Total Variation–biharmonic (TV^2–BH) model in which the TV method is used in combination with a fourth-order Laplacian diffusion term. The Euler–Lagrange equation is derived as a nonlinear fourth-order PDE and solved using appropriate numerical methods. The experience gained from using the TV^2–BH method shows that the proposed approach yields much better results in comparison with the standard inpainting methods due to the preservation of texture patterns and edge information, as well as homogeneous areas and staircase effect minimization. The soundness of the proposed model is duly proved through quantitative assessments based on Peak Signal-to-Noise Ratio (PSNR), Structural Similarity Index Measure (SSIM), and Mean Squared Error (MSE). The obtained results confirm that improved reconstruction performance can be achieved by the proposed model compared with classical TV, biharmonic, and TV^2 inpainting methods.

Keywords: image inpainting; laplacian operator; total variation; variational methods; fourth-order PDEs; biharmonic equation; anisotropic diffusion model; edge preservation; isophote lines

Check for updates

Academic Editor: Guillermo Valencia-Palomo

Received: 19 August 2026
Revised: 7 September 2026
Accepted: 9 September 2026
Published: 11 September 2026

Copyright: © 2026 by the authors. Licensee MDPI, Basel, Switzerland. This article is an open access article distributed under the terms and conditions of the Creative Commons Attribution (CC BY) license.

1. Introduction

In simple terms, image inpainting is a method of recovering missing, corrupted, or unwanted parts of an image by effectively using information from adjacent regions. Originally stemming from the restoration of damaged works of art or photographs, image inpainting has developed into a crucial research field in computer vision and image processing, serving various purposes such as removing objects, restoring images, and supporting applications in medicine, remote sensing, cinema post-production, and digital heritage conservation. Among the various methods developed for image inpainting, partial differential equation (PDE)-based methods are among the earliest and most mathematically rigorous frameworks.

In the year 2000, the first image inpainting technique was developed by Marcelo Bertalmío and Guillermo Sapiro. Their theory involved transferring image data from the

edges to the damaged areas, similar to what professional painters do [1]. The technique could fill in small sections of the image while preserving the geometric principles and continuous edges. Recently, researchers have enhanced the restoration process using PDE concepts.

Linear diffusion methods allow the information to be distributed through minor absent sections without much creation of artifacts at the edges (i.e., textures). In addition, nonlinear anisotropic diffusion models were developed thanks to the efforts of Pietro Perona and Jitendra Malik to restore images through a controlled diffusion process [2]. The above-mentioned methods create a diffusion process based on the local image structure from the boundary to the absent regions, while preserving edge information. Later, variational methods emerged in the field of PDE-based image inpainting. The Total Variation (TV) model was introduced by Leonid Rudin and colleagues through the development of image inpainting techniques [3]. The application of these methods is much broader than that of linear diffusion methods, as they preserve sharp edges and have been widely applied to image inpainting and other tasks. To control gradient artifacts commonly associated with second-order PDEs, researchers have either combined multiple second-order models [4] or introduced higher-order PDE models [5].

Curvature-driven diffusion (CDD) [6] and Euler–Elastica-based methods [7] use geometric information, such as curvature, to spread structures through missing regions. These models produce smoother transitions and improved edge continuation, particularly in images containing elongated structures and contours. Their ability to reconstruct geometric features made them particularly suitable for scratch removal and object deletion tasks. Another influential direction involved fluid dynamics-inspired models [8]. The Navier–Stokes inpainting generally treated image intensity as a fluid quantity and applied transport equations to spread isophotes through damaged areas in the image. These methods achieved perfect edge spread and structural protection but often collapsed due to high computational complexity. As a result, numerical efficiency for these methods will improve in subsequent studies while preserving restoration quality [9].

Over the last 10 years, various researchers have studied hybrid PDE models that incorporate diffusion, variational regularization, and shock-filtering techniques [10]. For example, in regularized diffusion-shock (RDS) models, the process of homogeneous diffusion is implemented via coherence-enhancing shock filters, which ultimately leads to successful completion of smoothing and enhancement of the borderline. The results showed an increase in restoration quality for images that contain significant directional characteristics and textures. Recent developments have focused on fractional-order PDEs, which are considered more flexible than traditional integer-order operators [11]. The application of fractional Laplacian regularization produces various non-local connections that help to create long-distance dependencies in the picture. Recently, a model of image inpainting has been proposed that is based on the combination of fractional Laplacian regularization and optimization based on the (L^p)-norm, thus showing better rates of preservation of pictures' structures and textures than other traditional methods based on PDEs.

A 2024 study introduced a mechanism-based inpainting method that learns differential equation representations from known image regions and uses them to reconstruct missing areas [12]. This framework demonstrated robustness and flexibility, particularly for scientific and structured image data. Recent research has further explored phase-field PDEs and Allen–Cahn-type equations for image inpainting. In 2025, an unconditionally stable numerical algorithm based on a penalized Allen–Cahn equation was proposed for binary image restoration, providing theoretical stability guarantees and an efficient numerical implementation [13,14]. Although deep learning approaches currently dominate the image inpainting literature, PDE-based methods remain highly relevant due to their strong

mathematical foundations, interpretability, and ability to preserve geometric structures. Modern research increasingly combines PDE models with machine learning techniques, creating hybrid frameworks that exploit both physical priors and data-driven representations. Recent reviews indicate that classical PDE methods remain important components of advanced image restoration systems and provide valuable theoretical guidance for the development of next-generation inpainting algorithms [15]. In summary, PDE-based image inpainting has evolved from classical diffusion equations to sophisticated models involving variational principles, curvature-driven flows, fractional operators, shock filters, and phase-field formulations [16]. Despite the remarkable success of deep neural networks, PDE approaches continue to offer robust, interpretable, and mathematically grounded solutions, particularly in applications where geometric fidelity and theoretical guarantees are essential [17].

The current paper addresses the question of image inpainting and proposes a TV^2–BH model that combines the TV^2 model [18] and the biharmonic regularization [19] to improve structural preservation and reduce artifacts in reconstructed image regions. The rest of the paper is given as follows: Section 2 presents the research methodology for image inpainting. Section 3 introduces the TV^2–BH method for reconstructing missing regions in color images. Section 4 displays the numerical results for the suggested technique and other methods. Section 5 discusses the results of applying the suggested method and its performance. Finally, Section 6 presents the outcomes and upcoming work.

2. Research Methodology

This section presents the components used in the proposed TV^2–BH technique. This work introduces the problem statement, the mathematical formulation of the TV^2–BH model, and the Euler–Lagrange equation and gradient flow equation.

2.1. Problem Statement

Let $\Omega \subseteq \mathbb{R}^2$ denote the image domain and let $D \subseteq \Omega$ represent the damaged or missing region to be reconstructed. The known image information is available on $\Omega - D$. Given a degraded image $f : \Omega \longrightarrow \mathbb{R}$, the objective of image inpainting is to recover an image $u : \Omega \longrightarrow \mathbb{R}$ that preserves geometric structures, edge continuity, and visual coherence within the missing region.

The objective is

$$u = \arg\min_u E(u), \tag{1}$$

where $E(u)$ is an energy functional that combines fidelity, fourth-order regularization, and biharmonic propagation.

Image inpainting aims to reconstruct missing or damaged regions while preserving the geometric structures and visual continuity of the original image. Classical first-order Total Variation models efficiently preserve sharp edges but often exhibit a gradient effect in smoothed areas. In contrast, biharmonic models produce smooth interpolations but tend to over-smooth edges and fine image texture.

To overcome these limitations, we propose the TV^2–BH model, which combines the edge-preserving capabilities of a TV^2 regularizer with the smoothing properties of biharmonic regularization. The proposed model aims to balance edge preservation, smooth surface reconstruction, and numerical stability.

2.2. Mathematical Formulation of the TV^2–BH Model

The proposed energy functional (1) is introduced as follows:

$$E(u) = E_f + E_{TV^2} + E_{BH}. \tag{2}$$

E_f represents the fidelity term, which is given as follows:

$$E_f = \frac{\lambda}{2}\int_{\Omega\setminus D}(u-f)^2 dx. \tag{3}$$

Outside the missing region D, the reconstructed image f should remain close to the observed image u.

E_{TV^2} is the functional of the TV^2, which is given as follows:

$$E_{TV^2} = \alpha\int_{\Omega}\|H(u)\|_F dx. \tag{4}$$

To know what $H(u)$ means and how it is found, see Appendix A.1.

Unlike classical TV regularization, the TV^2 functional penalizes second-order derivatives rather than first-order derivatives, thereby significantly reducing staircase artifacts while preserving curved structures.

E_{BH} is the biharmonic energy, which is defined as follows:

$$E_{BH} = \frac{\beta}{2}\int_{\Omega}(\Delta u)^2 dx, \tag{5}$$

where

$$\Delta u = u_{xx} + u_{yy},$$

is the Laplacian operator. This regularization promotes the following:

- Smooth surface interpolation;
- Higher-order continuity;
- Stable reconstruction in large missing regions;
- Oscillation suppression.

Combining the three terms yields the following:

$$E(u) = \frac{\lambda}{2}\int_{\Omega\setminus D}(u-f)^2 dx + \alpha\int_{\Omega}\|H(u)\|_F dx + \frac{\beta}{2}\int_{\Omega}(\Delta u)^2 dx, \tag{6}$$

where $\lambda > 0$ is the fidelity parameter, $\alpha > 0$ controls the TV^2, and $\beta > 0$ controls the biharmonic regularization.

2.3. Euler–Lagrange Equation and Gradient Flow Equation [20])

Taking the first variation of the energy functional (6) gives

$$\lambda\chi_{\Omega\setminus D}(u-f) + \alpha\nabla^2\cdot\left(\frac{H(u)}{\|H(u)\|_F}\right) + \beta\Delta^2 u = 0. \tag{7}$$

Here,

$$\Delta^2 u = \Delta(\Delta u),$$

is the biharmonic operator.

Note: To explain how we are applying the Euler–Lagrange equation to E_{TV^2}, see Appendix A.2.

For the proposed energy functional (2), the gradient flow is defined according to the steepest-descent convention

$$\frac{\partial u}{\partial t} = -\frac{\delta E}{\delta u} \tag{8}$$

To solve the minimization problem of (7) numerically, the steepest-descent convention for Equation (7) is applied according to Equation (8), as follows:

$$\frac{\partial u}{\partial t} = -\lambda \chi_{\Omega \setminus D}(u - f) - \alpha \nabla^2 \cdot \left(\frac{H(u^n)}{\|H(u^n)\|_F + \varepsilon} \right) + \beta \Delta^2 u. \tag{9}$$

This is a nonlinear fourth-order PDE. The steady-state solution of this evolution process is the minimizer of the proposed energy functional. The initial condition is

$$u(x, y, 0) = f(x, y).$$

Natural Neumann boundary conditions are imposed on the image boundary:

$$\begin{cases} \frac{\partial u}{\partial n} = 0 \\ \frac{\partial (\Delta u)}{\partial n} = 0 \end{cases} \qquad x, y \in \partial D.$$

This can be explained by the fact that the known values of the image are kept unchanged, while Neumann normal conditions are imposed on the outer limits to ensure the stability of the reconstruction and compatibility with the fourth-order nature of the biharmonic effect.

3. Semi-Implicit Numerical Scheme

For numerical implementation of Equation (8), the linear biharmonic term is treated implicitly, while the nonlinear TV^2 term is handled explicitly [21]. The time derivative is approximated using the backward difference, as seen below:

$$\frac{\partial u}{\partial t} \approx \frac{u^{n+1} - u^n}{\Delta t}.$$

Substituting into Equation (9) gives

$$\frac{u^{n+1} - u^n}{\Delta t} = -\lambda (u^n - f) - \alpha TV^2(u^n) + \beta \Delta^2 u^{n+1}, \tag{10}$$

where

$$TV^2(u^n) = \nabla^2 \cdot \left(\frac{H(u^n)}{\|H(u^n)\|_F + \varepsilon} \right).$$

where the Hessian matrix is divided component-wise by its Frobenius norm (plus a small regularization parameter (ε)). This is the form that is consistent with the Euler–Lagrange derivation and is the one you should use in both the mathematical formulation and the MATLAB implementation [22].

Notice that

- TV^2 is evaluated at time (n) (explicit);
- The biharmonic operator is evaluated at time $(n+1)$ (implicit).

This is why the method is called **semi-implicit**.

Multiplying by (Δt),

$$u^{n+1} - \beta \Delta t \Delta^2 u^{n+1} = u^n - \Delta t \left[\lambda (u^n - f) + \alpha TV^2(u^n) \right].$$

The semi-implicit discretization of Equation (10) is as follows:

$$(I - \beta \Delta t \Delta^2) u^{n+1} = u^n - \Delta t \left[\lambda (u^n - f) + \alpha TV^2(u^n) \right]. \tag{11}$$

Factorizing,

$$(I - \beta\Delta t\Delta^2)u^{n+1} = b^n,$$

where

$$b^n = u^n - \Delta t\Big[\lambda(u^n - f) + \alpha TV^2(u^n)\Big].$$

At each iteration, the output of Equation (10) computes u^{n+1}. Suppose the image has $N \times M$ pixels. Flatten it into a vector $u \in \mathbb{R}^{NM}$.

The discrete biharmonic operator becomes a sparse matrix $L \in \mathbb{R}^{NM\times NM}$. Then, using the implicit treatment,

$$(I - \beta\Delta tL)u^{n+1} = b^n, \tag{12}$$

allows much larger time steps because the dominant fourth-order diffusion is handled implicitly.

This is simply a linear system:

$$Au^{n+1} = b^n,$$

where

$$A = I - \beta\Delta tL.$$

Thus, the output of the semi-implicit step is **not a scalar**; it is the entire reconstructed image at the next time level. A completely explicit formulation of the fourth-order diffusion operator leads to a rather severe time-step restriction according to which

$$\Delta t = O\Big(h^4\Big),$$

which becomes increasingly restrictive when the spatial grid is refined. In order to remove this constraint, we conceived a semi-implicit scheme that treats the stiff fourth-order term implicitly. This way, the strict condition associated with the explicit CFL approaches becomes less stringent and allows using larger time steps but still keeps numerical stability. The value used $\Delta t = 0.1$, in practice, was selected through numerical stability testing.

3.1. Iterative Algorithm

For each iteration:

1. Start with the current estimate (u^n).
2. Compute image gradients.
3. Compute the Hessian matrix $H(u^n)$.
4. Compute the Frobenius norm of the Hessian $\|H(u)\|_F = \sqrt{u_{xx}^2 + 2u_{xy}^2 + u_{yy}^2 + \varepsilon}$.
5. Evaluate the nonlinear TV^2 operator $TV^2(u^n) = \nabla^2 \cdot \Big(\frac{H(u^n)}{\|H(u^n)\|_F + \varepsilon}\Big)$.
6. Assemble the right-hand side: $b^n = u^n - \Delta t\big[\lambda(u^n - f) + \alpha TV^2(u^n)\big]$.
7. Solve $\big(I - \beta\Delta t\Delta^2\big)u^{n+1} = b^n$.
8. Iterations continue until convergence: $\frac{\|u^{n+1} - u^n\|_2}{\max(\|u^n\|_2, \epsilon_0)} < 10^{-6}$, where ϵ_0 is a small positive number used to avoid division by zero.

If not converged, set $\big(u^n = u^{n+1}\big)$ and repeat, as seen in Figure 1.

Figure 1 displays the flowchart of the semi-implicit algorithm for solving the proposed (TV^2–BH) model.

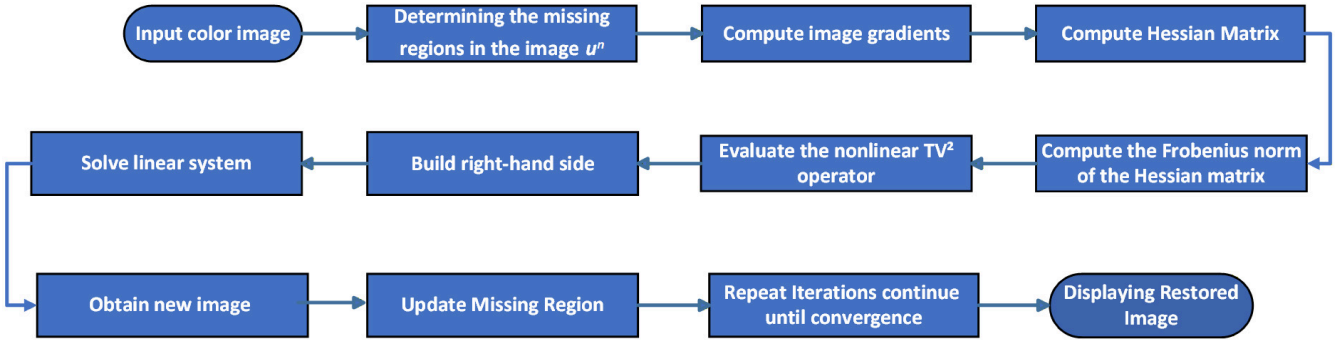


Figure 1. Flowchart of the semi-implicit algorithm.

3.2. Physical Interpretation

The update equation can be interpreted as the interaction of three competing effects:

Data fidelity term:

$$-\lambda(u - f).$$

Keeps the known pixels close to the original image.

2nd-order TV term:

$$-\alpha\nabla^2 \cdot \left(\frac{H(u)}{\|H(u)\|_F}\right).$$

Preserves edges while reducing staircase artifacts.

Biharmonic diffusion term:

$$+\beta\Delta^2 u.$$

Produces smooth interpolation inside missing regions and suppresses oscillations.

4. Experimental Results

To assess the effectiveness of the proposed TV^2–BH technique, several numerical experiments were conducted on 100 natural-color images from the Berkeley database [23], including low- and high-texture images, as illustrated in Figure 2. These images were chosen at different levels of texture and structure to evaluate the effectiveness of the TV^2–BH technique in restoring missing areas.

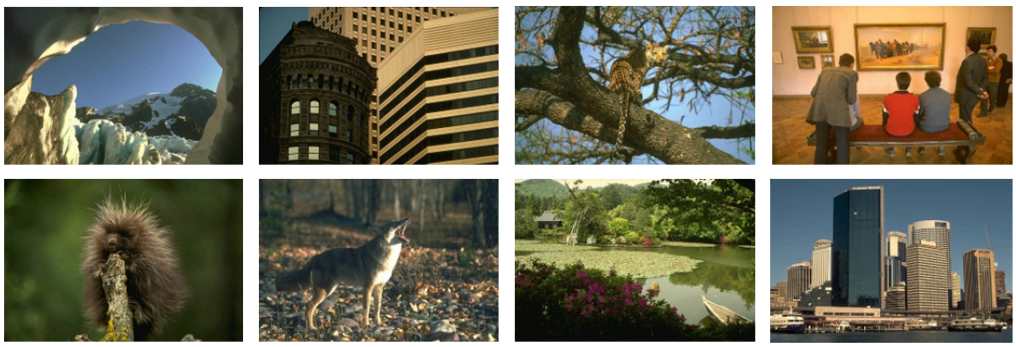


Figure 2. Example of 8 out of 100 color images.

The proposed TV^2–BH method is applied to restore lost areas of different sizes in color image data. Figure 3 displays six inpainting masks that illustrate six damaged regions in images.

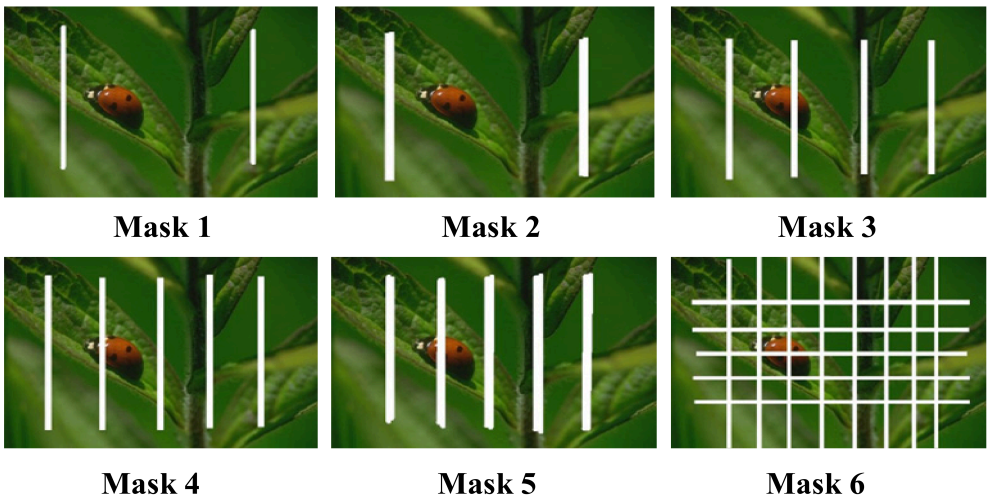


Figure 3. The same color image with six different inpainting domains.

Figure 3 shows six different inpainting domains (or masks). The sizes of the missing areas for these masks are shown in Table 3. The aim of the inpainting Mask1, Mask2, Mask3, Mask4, Mask5, and Mask6 domains is to evaluate the proposed method's ability to restore missing regions of different sizes using textures from neighboring areas. To evaluate the effectiveness of the proposed method, the TV^2–BH method was applied to these masks on over 100 images in the Berkeley database.

4.1. Performance Evaluation

To demonstrate the method's effectiveness, standard image quality criteria were used. To derive numerical results, image quality standards (SQMs) were compared with the outcomes achieved by the proposed TV^2–BH model and the other techniques: TV, biharmonic, and TV^2. Mean square error (MSE), peak signal-to-noise ratio (PSNR) [24], structural similarity index (SSIM) [25,26], and entropy [27] of original and inpainted images were among the measures, thus giving the numerical value of image distortion.

More specifically, in the context of considering u as the image being reconstructed and f as the original image, in calculating the quality of how completely an image was reconstructed, this process is performed using only the distance within the region of the mask; that is, D is given by:

$$\mathrm{MSE}_D = \frac{1}{|D|}\sum_{k=1}^{q}\sum_{i=1}^{n}\sum_{j=1}^{m}[u_k(i,j) - f_k(i,j)]^2 \tag{13}$$

where $q = 3$ is the number of color channels in the image, while n and m are the number of rows and columns in the channel image, thereby giving $D = n \times m \times q$. A better image quality is one where the error is lower, as is shown by the small MSE value. Hence, once MSE is calculated, the PSNR [24] is given as follows:

$$\mathrm{PSNR}_D = 10\log_{10}\left(\frac{\mathrm{MAX}^2}{\mathrm{MSE}}\right) \tag{14}$$

where MAX is the maximum intensity of the image, where less error corresponds to higher PSNR. PSNR and MSE have an inverse relationship.

SSIM [25,26] is a correlated measure of the Luminance L, Contrast C, and Structural S values of the original f and the image u being inpainted.

$$\mathrm{SSIM}_D = \left[L_D(u,\ f)^{\delta} \cdot C_D(u,\ f)^{\xi} \cdot S_D(u,\ f)^{\gamma} \right], \tag{15}$$

where

$$L_D(u,\ f) = \frac{2\mu_f \mu_u + c_1}{\mu_f^2 + \mu_u^2 + c_1},\ C_D(u,\ f) = \frac{2\sigma_f \sigma_u + c_2}{\sigma_f^2 + \sigma_u^2 + c_2},\ S_D(u,\ f) = \frac{2\sigma_{fu} + c_3}{\sigma_f \sigma_u + c_3},\ c_3 = c_2/2, \text{ and } \delta = \xi = \gamma = 1.$$

Then this is defined mathematically as follows:

$$\mathrm{SSIM}(u,\ f) = \frac{(2\mu_f \mu_u + c_1)(2\sigma_{fu} + c_2)}{(\mu_f^2 + \mu_u^2 + c_1)(\sigma_f^2 + \sigma_u^2 + c_2)}, \tag{16}$$

where (μ_f, σ_f) and $(\mu_{\ u}, \sigma_u)$ shows the mean and standard deviation of the images u and f, respectively; σ_{fu} is the covariance of u and f images; $c_1 = (k_1 h)^2, c_2 = (k_2 h)^2$ such that $k_1 = 0.01$, $k_2 = 0.03$, and $h = 2^{bits\ per\ pixel} - 1$. In this work, SSIM is computed over windows of size 8×8 in the missing region D and the outputs from the R, G, and B channels are then averaged. The SSIM value is a numeric representation that can vary between -1 and 1. The integer 1 can be achieved when there is no difference between the original and restored image. The maximum image quality is achieved when the error is minimal, and the SSIM value is 1.

Entropy [27] is defined as the quantitative measure of randomness or disorder of the image. The entropy of an inpainted image u is defined as follows:

$$\mathrm{Entr}(u) = -\sum_{i=1}^{n} \sum_{j=1}^{m} P_{u_{i,j}} \log_2 P_{u_{i,j}} \tag{17}$$

where $P_{u_{i,j}}$ is the probability of pixel values (i.e., the distribution of element values), and $\log_2$ is the base-2 logarithm function applied. To calculate the entropy of the original image f, the same Equation (17) is applied. Hence, in general, high entropy denotes less information about the uncertainty of an image, while low entropy denotes more information about the uncertainty of an image. The same measurement is applied to the inpainted regions for the cases of different inpainting methods. The best outcome is the entropy measurement when the entropy of the inpainted image u is equal to the entropy of the original image f. The most efficient algorithm based on entropy values is the one with the minimum difference between the entropy value of the restored image and the original image.

The comparison of these quantitative measures allowed for evaluating the effectiveness and success of the model in regaining lost regions in images, along with measuring the time needed to obtain the results. The TV^2–BH technique of regaining lost regions in images was implemented in MATLAB (version R2022a) and run on a laptop with an Intel Core i5-10210U processor of 2.11 GHz (Huawei) and 1.60 GHz L2 memory of 1.60 GHz along with 8 GB RAM. The time of the results was measured.

To ensure that the quantitative measures directly reflect the quality of the reconstructed regions, all objective metrics are computed exclusively within the missing region (D). The pixels reconstructed in area (D) are compared with the corresponding pixels in the intact image, but known pixels outside area (D) are not included in the metric calculation. MSE, PSNR, and SSIM can measure the reconstruction quality in the missing area. This approach prevents potential attenuation of reconstruction errors, as would have been the case if the whole image had been taken into account, because pixels outside of the affected area are not modified during the inpainting process.

4.2. Testing Parameters and Experiments

For the proposed TV^2–BH model (6), there is **no universally optimal** choice of α, β, and λ. The best values depend on the size of the missing region, the image texture, the noise level, and the image resolution. In this study, the effect of the values λ, α, and β on the performance of the TV^2–BH model in recovering the missing regions in an image is studied.

However, based on the behavior of 4th-order variational models and practical experience with TV^2 and biharmonic regularization, the following values provide an excellent starting point for **normalized images in [0, 1]**. Therefore, we use two scenarios: firstly, the values of λ, β, and α are chosen differently, as shown in Table 1. Secondly, we study the values of λ, β, and α with the TV^2–BH model for recovering different missing regions, as seen in Table 3.

Table 1. Different values of parameters λ, α, and β.

λ Parameter	α Parameter	β Parameter
2	0.05	0.01
5	0.1	0.05
10	0.5	0
15	1	0.1
20	2	0.5

Scenario I: Different values of λ, α, and β are used by applying the TV^2–BH model for recovering the missing region in mask 1, as shown in Table 1.

This study was conducted on 100 color images, with 300 iterations. The mean values of MSE, SSIM, PSNR, entropy, and the time required to obtain results using the TV^2–BH model are introduced in Table 2.

Table 2. SQMs for recovering missing regions in mask 1, iteration = 300, obtained using the TV^2–BH model at different parameter values λ, α, and β.

Parameters	MSE	PSNR	SSIM	Entr (f)	Entr (u)	Time (s)
$\lambda = 2$ $\alpha = 0.05$, $\beta = 0.05$	45.85381	31.51705	0.412134	6.682838	6.080597	21.49935
$\lambda = 5$ $\alpha = 0.1$, $\beta = 0.02$	5.437109	40.77712	0.833003	6.682838	6.478285	60.84529
$\lambda = 10$ $\alpha = 0.5$, $\beta = 0$	18.28849	35.50903	0.664196	6.682838	5.877241	42.65167
$\lambda = 15$ $\alpha = 1$, $\beta = 0.1$	21.93972	34.71849	0.579689	6.682838	6.161192	58.65872
$\lambda = 20$ $\alpha = 2$, $\beta = 0.5$	13.63483	36.78431	0.559309	6.682838	6.254559	74.15168

We found $\lambda = 5, \alpha = 0.1,$ and $\beta = 0.02$. These values generally provide a good balance between edge preservation, smooth continuation, and fidelity to the known pixels. Other

values of the parameters λ, α, and β made the results of applying the TV^2–BH model not promising, as seen in Table 2.

In Scenario II, we focused on comparing how the selection of parameters λ, α, and β may affect the performance of this TV^2–BH method in reaching optimum results for missing regions of different sizes. Table 3 shows the sizes of the missing regions considered.

Table 3. The values of parameters λ, β, and α for different missing areas.

Masks	Missing Area	λ Parameter	α Parameter	β Parameter
Mask 1	<5%	7	0.09	0.01
Mask 2	5–10%	6	0.08	0.01
Mask 3	10–20%	5	0.1	0.02
Mask 4	20–30%	4	0.13	0.03
Mask 5	30–40%	3	0.15	0.04
Mask 6	>40%	2	0.2	0.05

In this experiment, we test each missing area individually in separate tests with the TV^2–BH model under different parameter values for λ, α, and β. This study was conducted on 100 color images. The mean values of MSE, SSIM, PSNR, entropy, and the time required to obtain results using the TV^2–BH model are introduced in Table 4, which summarizes the results of these experiments, showing the most successful values of λ, α, and β for the proposed TV^2–BH method for each missing region in masks 1, 2, 3, 4, 5, and 6.

Table 4. SQMs for recovering different missing regions in images, obtained using the TV^2–BH model at the parameter values of parameters λ, β, and α.

Masks	Parameters	MSE	PSNR	SSIM	Entr (f)	Entr (u)	Time (s)	Iterations
Mask 1	$\lambda = 7$ $\alpha = 0.09$, $\beta = 0.01$	5.437109	40.77712	0.833003	6.682838	6.478285	60.84529	300
Mask 2	$\lambda = 6$ $\alpha = 0.08$, $\beta = 0.01$	8.947177	38.61394	0.796154	6.682838	6.220742	73.15621	500
Mask 3	$\lambda = 5$ $\alpha = 0.1$, $\beta = 0.02$	12.18921	37.27105	0.605243	6.682838	6.290969	87.05397	700
Mask 4	$\lambda = 4$ $\alpha = 0.13$, $\beta = 0.03$	16.18808	36.04082	0.795467	6.682838	6.182749	92.18123	800
Mask 5	$\lambda = 3$ $\alpha = 0.15$, $\beta = 0.04$	18.91693	35.36231	0.637561	6.682838	5.979385	112.8685	1000
Mask 6	$\lambda = 2$ $\alpha = 0.2$, $\beta = 0.05$	21.93972	34.71849	0.679689	6.682838	5.861192	124.1143	1200

The results of the TV^2–BH model were promising, as seen in Table 4. The results were stable, and the model's performance was good for the values of the parameters λ, α, and β in recovering the missing regions (6 Masks) in the image.

The λ fidelity parameter controls how strongly the reconstructed image matches the known pixels. When the λ parameter is a small value, applying the TV^2–BH model to

recover missing regions in an image produces excessive diffusion and a loss of image contrast. When the λ parameter is a large value, applying the TV^2–BH model to recover missing regions in an image produces a solution that remains too close to the damaged image and has slower propagation into large missing regions.

The α second-order TV regularization parameter controls the strength of the Hessian-based TV^2 term. When the α parameter is a small value (<0.05), applying the TV^2–BH model to recover missing regions in an image produces weak regularization, noisy reconstruction, and discontinuous isophotes. When the α parameter is a large value (>0.20), applying the TV^2–BH model to recover missing regions in an image produces stronger edge preservation, possible over-smoothing of textures, and slower convergence.

The β biharmonic regularization parameter governs smooth interpolation inside the missing region. When the β parameter is a small value, applying the TV^2–BH model to recover missing regions in an image produces insufficient diffusion, and oscillations may remain. When the β parameter is a large value, applying the TV^2–BH model to recover missing regions in an image produces excessive smoothing and blurred edges. Finally, we recommend values for different inpainting problems, as given in Table 4. We found that for larger damaged regions, increasing α and β while slightly decreasing λ generally improves propagation into the missing area. These values provide a good compromise between preserving edges (TV^2 term), ensuring smooth continuation across missing regions (biharmonic term), and maintaining fidelity to the known image data. They are an appropriate baseline before optimizing parameters for a specific dataset.

4.3. Image Inpainting Experiments

The effectiveness of the TV^2–BH method was evaluated both qualitatively and quantitatively. The qualitative evaluation measures the visual quality of the restored images, while the quantitative evaluation relies on statistical measures, as previously mentioned.

Figures 4–9 compare the proposed TV^2–BH method with three image restoration techniques for missing area recovery: TV, biharmonic, and TV^2. Figures 4 and 5 show the results of restoring small damaged areas in several typical nature photographs. The image quality obtained here is typical for the majority of the tested images.

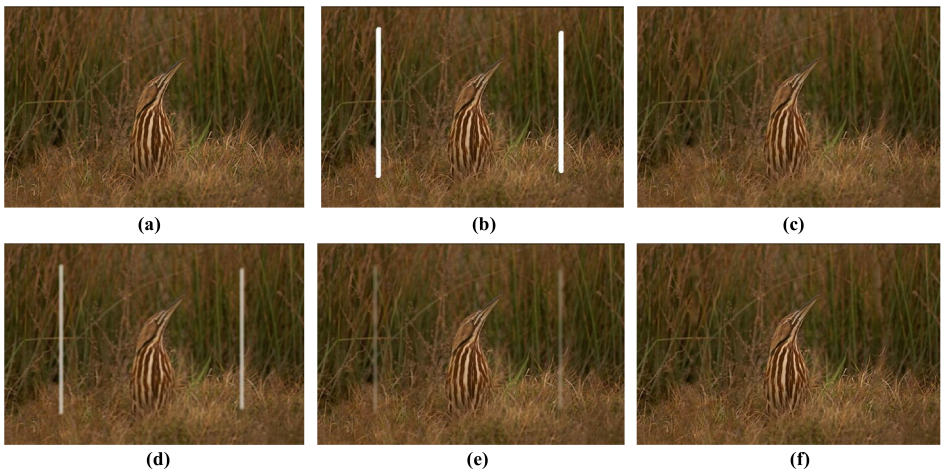


Figure 4. Inpainting a **Mask 1** image. (**a**) Reference image, (**b**) reference image with a mask, (**c**–**f**) reconstructed images via TV^2–BH, TV, biharmonic, and TV^2 techniques, respectively.

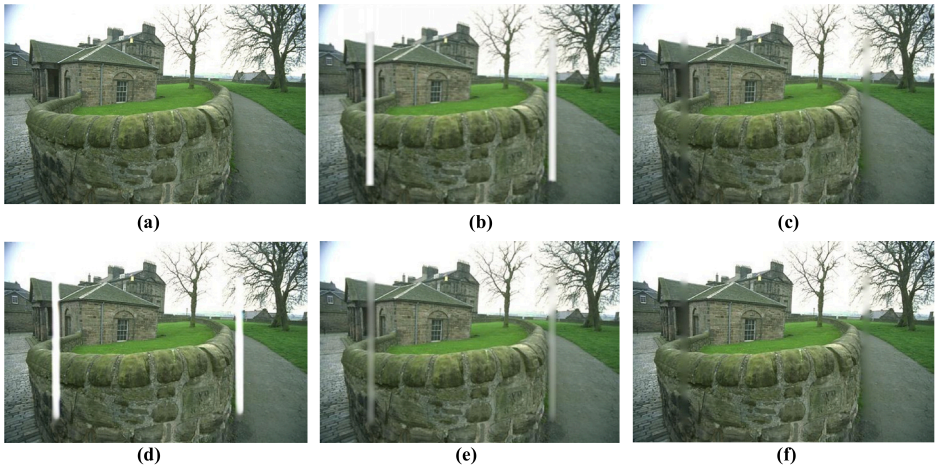


Figure 5. Inpainting a **Mask 2** image. (**a**) Reference image, (**b**) reference image with a mask, (**c**–**f**) reconstructed images via TV^2–BH, TV, biharmonic, and TV^2 techniques, respectively.

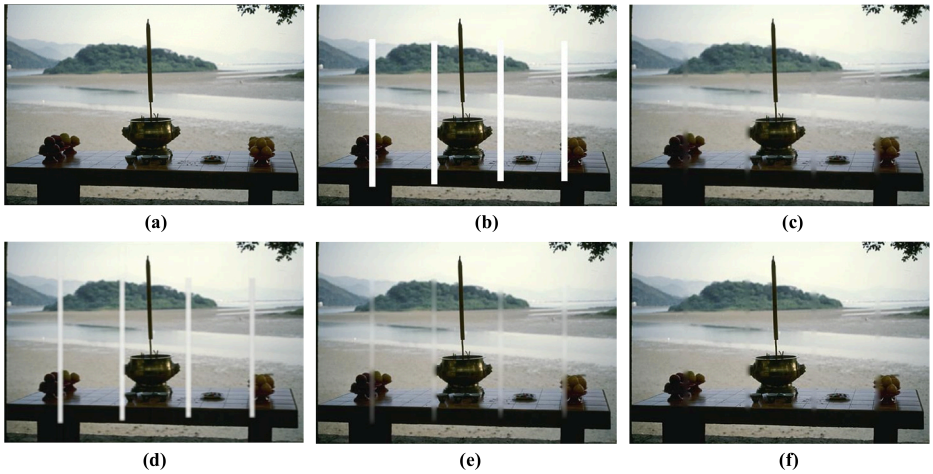


Figure 6. Inpainting a **Mask 3** image. (**a**) Reference image, (**b**) reference image with a mask, (**c**–**f**) reconstructed images via TV^2–BH, TV, biharmonic, and TV^2 techniques, respectively.

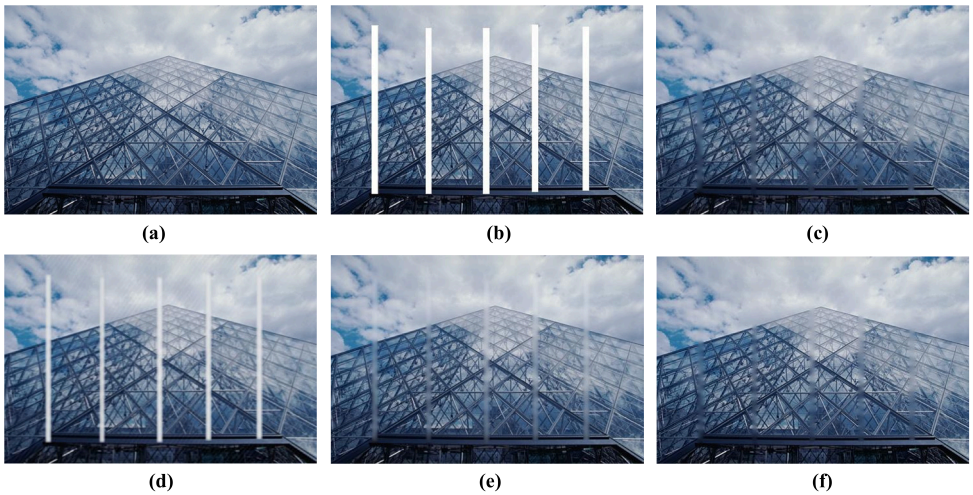


Figure 7. Inpainting a **Mask 4** image. (**a**) Reference image, (**b**) reference image with a mask, (**c**–**f**) reconstructed images via TV^2–BH, TV, biharmonic, and TV^2 techniques, respectively.

Figures 6–9 show the results of restoring different sizes of missing areas in some standard color images. The image quality shown here is typical of most of the images examined.

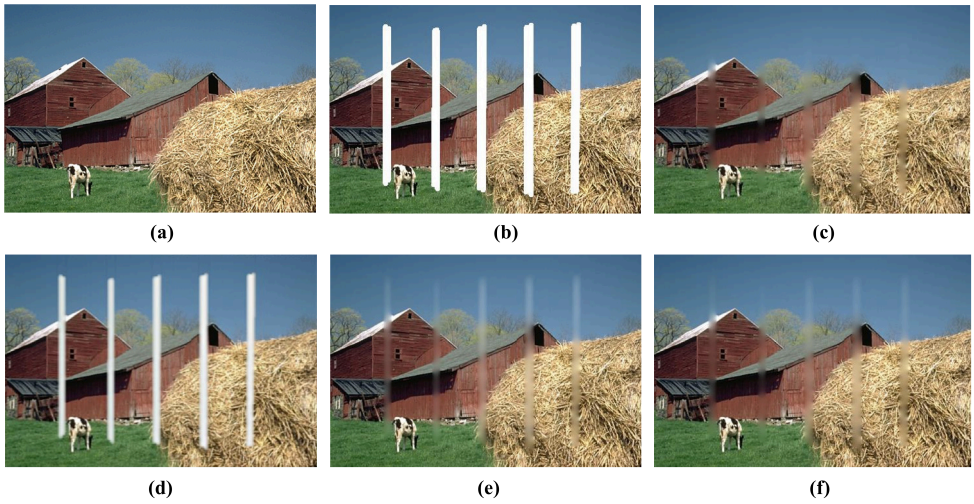


Figure 8. Inpainting a **Mask 5** image. (**a**) Reference image, (**b**) reference image with a mask, (**c**–**f**) reconstructed images via TV^2–BH, TV, biharmonic, and TV^2 techniques, respectively.

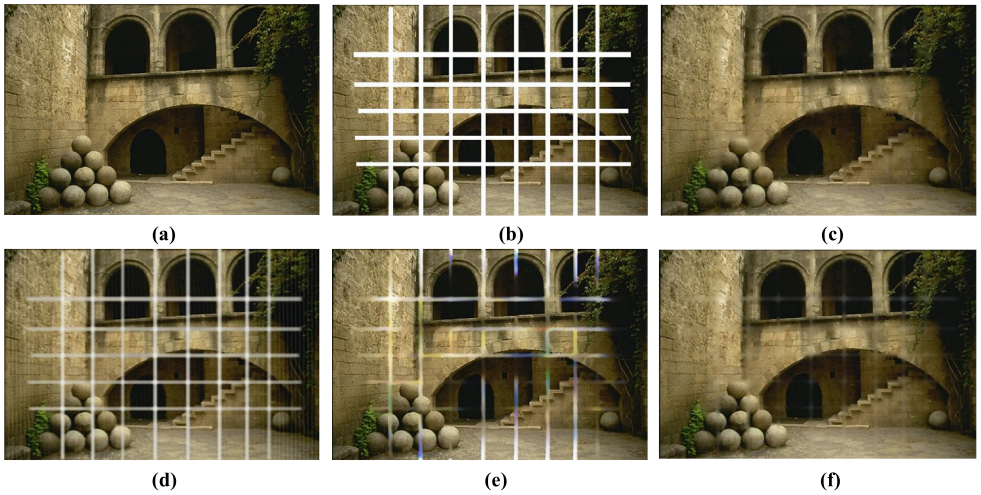


Figure 9. Inpainting a **Mask 6** image. (**a**) Reference image, (**b**) reference image with a mask, (**c**–**f**) reconstructed images via TV^2–BH, TV, biharmonic, and TV^2 techniques, respectively.

As depicted in Figures 4–9, the proposed TV^2–BH technique clearly outperforms the established TV method, the biharmonic method, and the TV^2 method. From a qualitative point of view, the images produced using the TV^2–BH model show better visual quality, as they maintain image structure and reconstruct missing parts of the image. The values of the parameters λ, β, and α shown in Table 4 were used, corresponding to each mask, and were applied to all images in the experiments. Thus, the parameter values differed across masks, as shown in Table 4. The mean values of MSE, SSIM, PSNR, entropy, and the time required to obtain results using the TV^2–BH model and other models in six inpainting domains are introduced in Table 5.

Table 5. SQMs using TV^2–BH, TV, biharmonic, and TV^2 techniques for **masks 1–6**.

Masks	Techniques	MSE	PSNR	SSIM	Entr (f)	Entr (u)	Time (s)
Mask 1	**TV**	13.63483	36.78431	0.459309	6.682838	5.054559	35.77331
	Biharmonic	9.964226	38.14637	0.541434	6.682838	6.877395	56.17674
	TV^2	7.372634	39.45458	0.621471	6.682838	6.930611	53.57771
	TV^2–BH	5.437109	40.77712	0.833003	6.682838	6.478285	60.84529

Table 5. *Cont.*

Masks	Techniques	MSE	PSNR	SSIM	Entr (f)	Entr (u)	Time (s)
Mask 2	**TV**	20.30828	35.05407	0.485659	6.682838	6.531704	42.65167
	Biharmonic	15.65645	36.18388	0.558369	6.682838	5.587834	535.3313
	TV^2	10.49377	37.92149	0.639993	6.682838	5.985517	69.86852
	TV^2–BH	8.947177	38.61394	0.796154	6.682838	6.220742	73.15621
Mask 3	**TV**	25.66941	34.03664	0.404171	6.682838	5.146459	47.21961
	Biharmonic	22.47783	34.61326	0.559449	6.682838	5.048408	64.61391
	TV^2	19.92924	35.13593	0.593346	6.682838	4.231406	53.00885
	TV^2–BH	12.18921	37.27105	0.605243	6.682838	6.290969	87.05397
Mask 4	**TV**	30.79894	33.24545	0.552292	6.682838	6.093909	71.52598
	Biharmonic	26.98189	33.82008	0.644632	6.682838	6.152734	75.96307
	TV^2	22.94426	34.52406	0.502416	6.682838	5.288017	86.02051
	TV^2–BH	16.18808	36.04082	0.795467	6.682838	6.182749	92.18123
Mask 5	**TV**	32.96402	32.95044	0.486243	6.682838	5.578011	81.08677
	Biharmonic	29.35718	33.45366	0.593554	6.682838	7.722488	92.09922
	TV^2	25.96471	33.98697	0.501013	6.682838	7.647125	102.4687
	TV^2–BH	18.91693	35.36231	0.637561	6.682838	5.979385	112.8685
Mask 6	**TV**	35.14308	32.67245	0.433063	6.682838	7.380378	93.99247
	Biharmonic	28.77424	33.54077	0.585157	6.682838	7.982572	102.1594
	TV^2	23.50859	34.41854	0.628056	6.682838	5.814576	112.2158
	TV^2–BH	21.93972	34.71849	0.679689	6.682838	5.861192	124.1143

5. Discussion

Table 5 presents the average values for MSE, SSIM, PSNR, entropy, and computation time obtained using different methods. Based on the observations, it is clear that the proposed scheme TV^2–BH achieves better inpainting performance than those of TV, biharmonic, and TV^2 methods across all types of missing areas. The above conclusions specifically indicate that the proposed method achieves greater accuracy in the recovery of structural and textural features of the damaged areas.

The observations made from Table 5 suggest that with respect to the use of the TV^2–BH method, higher PSNR values and lower values of MSE are achieved. This indicates that the resulting picture has survived and is almost identical to the original. In addition, the SSIM values provided by the method are comparatively very close to 1, which is an indication of its capability to retain the structural similarity. The values of entropy also tend to match those of the original pictures.

Nevertheless, the TV^2–BH method requires more computational time than the TV, biharmonic, and TV^2 methods when applied to color images. This time-consuming process arises from the combination of the terms of TV^2 and biharmonic regularization, resulting in a complex optimization problem that requires a larger number of iterations. However, the better reconstruction and preservation of structures and textures in the image support the idea of the effectiveness of the TV^2–BH model.

The main advantages of the proposed model are as follows:

- Preserves sharp edges using TV^2.
- Eliminates staircase artifacts commonly produced by first-order TV models.

- The TV^2–BH model produces smoother image surfaces through Biharmonic regularization.
- Reconstruction quality in regions with large missing values was improved.
- A semi-implicit time discretization improved numerical stability.
- Edge preservation and smooth interpolation are naturally balanced.

6. Conclusions and Future Work

The novel TV^2–BH model was introduced by combining nonlinear Hessian-based regularization with linear biharmonic smoothing in a unified variational framework. Its main contributions include a new variational energy that combines TV^2 and biharmonic regularization. This model simultaneously reconstructs image structures and a smooth surface. A semi-implicit numerical method was implemented for the TV^2–BH model, which reduced staircase artifacts compared with first-order TV methods. A mathematically consistent framework suitable for finite-difference discretization and iterative optimization was developed. Signal quality metrics (SQMs) were used to evaluate the results of various numerical experiments with the proposed TV^2–BH model and to demonstrate its effectiveness: MSE, PSNR, SSIM, and entropy. These metrics show that the proposed TV^2–BH method outperforms TV, biharmonic, and TV^2 methods in handling different types of missing regions without compromising efficiency.

In conclusion, both structural and textural information in the damaged areas of color images have been effectively reconstructed by the innovative TV^2–BH method. In the future, the proposed model can be further developed by introducing adaptive or anisotropic regularization. Various datasets will also be used to evaluate the effectiveness of the proposed TV^2–BH method through direct comparison with a wider range of contemporary learning-based approaches. Conversely, a TV^2–BH model can be applied with different approaches to develop a new hybrid strategy for recovering missing areas in images. Free-form and irregular masks are therefore an important direction for future work.

Author Contributions: Conceptualization, A.K.A.-J., A.A.L. and D.L.; methodology, A.K.A.-J. and A.A.L.; software, A.K.A.-J. and A.A.L.; validation, A.K.A.-J., A.A.L. and D.L.; formal analysis, A.K.A.-J. and A.A.L.; investigation, A.K.A.-J., A.A.L. and D.L.; resources, A.K.A.-J. and A.A.L.; data curation, A.K.A.-J. and A.A.L.; writing—original draft preparation, A.K.A.-J. and A.A.L.; writing—review and editing, A.K.A.-J., A.A.L. and D.L.; visualization, A.K.A.-J. and A.A.L.; supervision, A.K.A.-J. and A.A.L.; project administration, A.K.A.-J. and A.A.L. All authors have read and agreed to the published version of the manuscript.

Funding: This work was supported and funded by the University of Oradea, Romania.

Data Availability Statement: The images used in this research are part of the open-access dataset created by Arbelaez et al. [23] in 2007. This means that the authors cannot claim ownership of the original image dataset or the right to distribute it. All images presented in this study were used for research and educational purposes only, and all copyright conditions established by the original dataset creators were followed.

Acknowledgments: We thank all participants for their help in the phases of the research design and in generating the dataset.

Conflicts of Interest: The authors declare no conflicts of interest.

Abbreviations

The following abbreviations are used in this manuscript:

PDE	Partial Differential Equation
TV	Total Variation
TV^2	Second Total Variation

BH	Biharmonic Model
TV^2-BH	Second Total Variation- Biharmonic Model
MSE	Mean Squared Error
PSNR	Peak Signal-to-Noise Ratio
SSIM	Structural Similarity
RDS	Regularized Diffusion-Shock
CDD	Curvature-Driven Diffusion
SQMs	Image Quality Standards

Appendix A

Appendix A.1. Hessian Matrix of Image u

Where the gradient of image u is defined as follows:

$$\nabla u = \begin{bmatrix} u_x \\ u_y \end{bmatrix}.$$

The gradient of the image is defined as follows:

$$\nabla(\nabla u) = \nabla^2 u = \begin{bmatrix} u_{xx} & u_{xy} \\ u_{yx} & u_{yy} \end{bmatrix}.$$

Then

$$\nabla(\nabla u) = \nabla^2 u = H(u).$$

where $H(u)$ is the Hessian matrix of the image; the Frobenius norm is used for second derivatives, as below:

$$\|H(u)\|_F = \sqrt{u_{xx}^2 + 2u_{xy}^2 + u_{yy}^2 + \varepsilon},$$

since

$$u_{xy} = u_{yx},$$

Because the Hessian is symmetric, $(\varepsilon > 0)$ is a small positive constant introduced to avoid division by zero. The Hessian describes local curvature, edge bending, and surface shape. For image processing: u_{xx} measures curvature in the x-direction, u_{yy} measures curvature in the y-direction, and u_{xy} measures mixed curvature.

Appendix A.2. Euler-Lagrange Equation E_{TV^2}

To explain how we are applying the Euler–Lagrange equation to E_{TV^2}, we found as follows:

Define

$$\Phi = \sqrt{\|H(u)\|_F^2 + \varepsilon}.$$

Then

$$E_{TV^2} = \int_\Omega \Phi dx.$$

Differentiation gives

$$\delta E = \int_\Omega \frac{u_{xx}v_{xx} + 2u_{xy}v_{xy} + u_{yy}v_{yy}}{\Phi} dx.$$

This expression contains second derivatives of v. Applying integration by parts twice transfers derivatives from v to u. The resulting Euler–Lagrange equation is

$$\frac{\partial^2}{\partial x^2}\left(\frac{u_{xx}}{\Phi}\right) + 2\frac{\partial^2}{\partial x \partial y}\left(\frac{u_{xy}}{\Phi}\right) + \frac{\partial^2}{\partial y^2}\left(\frac{u_{yy}}{\Phi}\right) = 0.$$

In compact notation, the double-divergence operator can be expressed as

$$\nabla^2 \cdot \left(\frac{H(u^n)}{\|H(u^n)\|_F + \varepsilon} \right) = 0.$$

References

1. Bertalmío, M.; Sapiro, G.; Caselles, V.; Ballester, C. Image inpainting. In *Proceedings of the 27th Annual Conference on Computer Graphics and Interactive Techniques*; ACM Press: New York, NY, USA; Addison-Wesley Publishing Co.: Boston, MA, USA, 2000. [CrossRef]
2. Perona, P.; Takahiro, S.; Jitendra, M. Anisotropic diffusion. In *Geometry-Driven Diffusion in Computer Vision*; Springer: Dordrecht, The Netherlands, 1994; pp. 73–92. [CrossRef]
3. Rudin, L.I.; Stanley, O.; Emad, F. Nonlinear total variation-based noise removal algorithms. *Phys. D Nonlinear Phenom.* **1992**, *60*, 259–268. [CrossRef]
4. Ajberi, A.K.A.; Jawad, Z.R. A Novel Total Variation Model for Image Denoising with Different Types of Noise. *Iraqi J. Sci.* **2025**, *66*, 3907–3920. [CrossRef]
5. Zhao, D.-H.; Lai-Sheng, W. A fourth-order partial differential equation model from the Weber's total variation for image restoration. In *Proceedings of the 2011 3rd International Conference on Advanced Computer Control*; IEEE: Piscataway, NJ, USA, 2011. [CrossRef]
6. Chan, T.F.; Shen, J. Nontexture inpainting by curvature-driven diffusions. *J. Vis. Commun. Image Represent.* **2001**, *12*, 436–449. [CrossRef]
7. Shen, J.; Chan, T.F. Mathematical models for local nontexture inpaintings. *SIAM J. Appl. Math.* **2002**, *62*, 1019–1043. [CrossRef]
8. Bertozzi, A.L.; Esedoglu, S.; Gillette, A. Inpainting of binary images using the Cahn–Hilliard equation. *IEEE Trans. Image Process.* **2006**, *16*, 285–291. [CrossRef] [PubMed]
9. Ebadi, M.J.; Ebrahimi, A. Video Data Compression by Progressive Iterative Approximation. *Int. J. Interact. Multimed. Artif. Intell.* **2021**, *6*, 189–195. [CrossRef]
10. Schaefer, K.; Weickert, J. Regularised Diffusion–Shock Inpainting. *J. Math. Imaging Vis.* **2024**, *66*, 447–463. [CrossRef] [PubMed]
11. Yuan, H.; Su, W.; Lian, X.; Yao, Z.-A.; Hu, D. Image Inpainting with Fractional Laplacian Regularization: An Lp Norm Approach. *Mathematics* **2025**, *13*, 2254. [CrossRef]
12. Su, S.; Yang, J. Unconditionally Stable Algorithm with Unique Solvability for Image Inpainting Using a Penalized Allen–Cahn Equation. *Commun. Nonlinear Sci. Numer. Simul.* **2025**, *142*, 108503. [CrossRef]
13. Luo, X.; Chen, Y.; Cheng, J.; Sun, Z. A Mechanism-Based Method for Image Inpainting. *Appl. Math. Lett.* **2024**, *154*, 109113. [CrossRef]
14. Haq, M.U.; Haq, S.; Ali, I.; Ebadi, M.J. Approximate Solution of PHI-Four and Allen–Cahn Equations Using Non-Polynomial Spline Technique. *Mathematics* **2024**, *12*, 798. [CrossRef]
15. Halim, A.; Rohim, A.; Kumar, B.V.R.; Saha, R. A Fractional Image Inpainting Model Using a Variant of Mumford–Shah Model. *Multimed. Tools Appl.* **2025**, *84*, 37975–37996. [CrossRef]
16. Elharrouss, O.; Damseh, R.; Belkacem, A.N.; Badidi, E.; Lakas, A. Transformer-Based Image and Video Inpainting: Current Challenges and Future Directions. *Artif. Intell. Rev.* **2025**, *58*, 124. [CrossRef]
17. Menéndez, A.G. Physics Meets Pixels: PDE Models in Image Processing. *arXiv* **2024**. [CrossRef]
18. Marius, L.; Xue-Cheng, T. Iterative image restoration combining total variation minimization and a second-order functional. *Int. J. Comput. Vis.* **2006**, *66*, 5–18. [CrossRef]
19. Wen, Y.; Vese, L.A.; Shi, K.; Guo, Z.; Sun, J. Nonlocal adaptive biharmonic regularizer for image restoration. *J. Math. Imaging Vis.* **2023**, *65*, 453–471. [CrossRef]
20. Chan, T.F.; Shen, J.; Vese, L. Variational PDE models in image processing. *Not. AMS* **2003**, *50*, 14–26.
21. Karol, M.; Ramarosy, M. Semi-implicit finite volume scheme for solving nonlinear diffusion equations in image processing. *Numer. Math.* **2001**, *89*, 561–590. [CrossRef]
22. Li, J.; Chen, Y.T. *Computational Partial Differential Equations Using MATLAB®*; CRC Press: Boca Raton, FL, USA, 2019.
23. Arbelaez, P.; Fowlkes, C.; Pablo, D.M. The Berkeley Segmentation Dataset and Benchmark. 2007. Available online: https://davidstutz.github.io/superpixel-benchmark/md_docs_DATASETS.html (accessed on 1 September 2011).
24. Yang, Y.; Lei, Z.; Li, C. No-Reference Image Quality Assessment Combining Swin-Transformer and Natural Scene Statistics. *Sensors* **2024**, *24*, 5221. [CrossRef] [PubMed]
25. Chen, Z.; Du, J.; Li, J.; Lv, H. MDFN: Enhancing Power Grid Image Quality Assessment via Multi-Dimension Distortion Feature. *Sensors* **2025**, *25*, 3414. [CrossRef] [PubMed]

26. Raigonda, M.R. Signature Verification System Using SSIM in Image Processing. *J. Sci. Res. Technol.* **2024**, *2*, 5–11. [CrossRef]
27. Li, Y.; Chao, X. Distance-Entropy: An Effective Indicator for Selecting Informative Data. *Front. Plant Sci.* **2022**, *12*, 818895. [CrossRef] [PubMed]

Disclaimer/Publisher's Note: The statements, opinions and data contained in all publications are solely those of the individual author(s) and contributor(s) and not of MDPI and/or the editor(s). MDPI and/or the editor(s) disclaim responsibility for any injury to people or property resulting from any ideas, methods, instructions or products referred to in the content.